Argonne NATIONAL LABORATORY

ANL-19/49

Thermal Test of 29mm and 12mm Targets

Experimental Operations and Facilities Division

ANL-19/49

Thermal Test of 29mm and 12mm Targets

by
J. Bailey, R. Gromov, T. Petersen, and S. Chemerisov
Experimental Operations and Facilities Division, Argonne National Laboratory

September 2019

Table of Contents

Tables

Figures

Figures (Cont.)

This page intentionally left blank.

Introduction

NorthStar medical isotopes are planning to produce important medical radioisotope molybdenum-99 (Mo-99) through photonuclear reaction on molybdenum-100 (Mo-100). In this approach, multiple thin disks of enriched molybdenum metal will be bombarded with a 40-MeV electron beam. Because enriched Mo-100 is expensive, we intend to use as much beam power as possible to achieve maximum production yield and minimize the size of the target. This requirement leads to very high beam power density (heat deposition in the target), which sets challenging requirements for cooling. Together with scientists at Los Alamos National Laboratory, a team at Argonne National Laboratory has developed and demonstrated a cooling approach using pressurized helium, which allows for efficient heat removal.[1, 2] One of the challenges in this approach is the management of the heat load on the target window. The target window separates the high-pressure helium atmosphere inside the target from the vacuum in the beamline so it is constantly under stress from differential pressure. Also, the window is cooled only by the helium gas flow from one side, making the window design challenging. To validate calculation models, the team performed a series of tests at Argonne's Low Energy Accelerator Facility (LEAF).[3-6] This report describes additional tests for two target designs: a full-scale target 29 millimeters in diameter and a scaled-down version, 12 millimeters in diameter. We compared the results of the window temperature measurements and cooling system parameters obtained in the experiments with those predicted by analytical calculations and Computation Flow Dynamic (CFD) simulations. Results of the experiments and calculations are presented below.

Experimental Setup Description

NorthStar target window thermal tests were performed at Argonne's LEAF 55 MeV Linac on the "zero-degree"-line in the experimental cell. Beam energy was 30MeV for the 29mm window and 40MeV for the 12mm window. Maximum average beam power was 20kW, limited by the cooling capacity of the helium-cooling system. During the time of irradiation, the team continuously logged all of the Linac's parameters. The most important instruments for experimental data acquisition were the Basler™ Optical Transitional Radiation camera (OTR-camera), the Flir™ Infra-Red camera (IR camera), and the Beam Current Monitors (BCM) (Figure 1. Helium gas flow at up to 300 psi pressure was supplied by the helium cooling system. A set of thermocouples was used for direct temperature measurement of helium, target disks, and a beam dump.

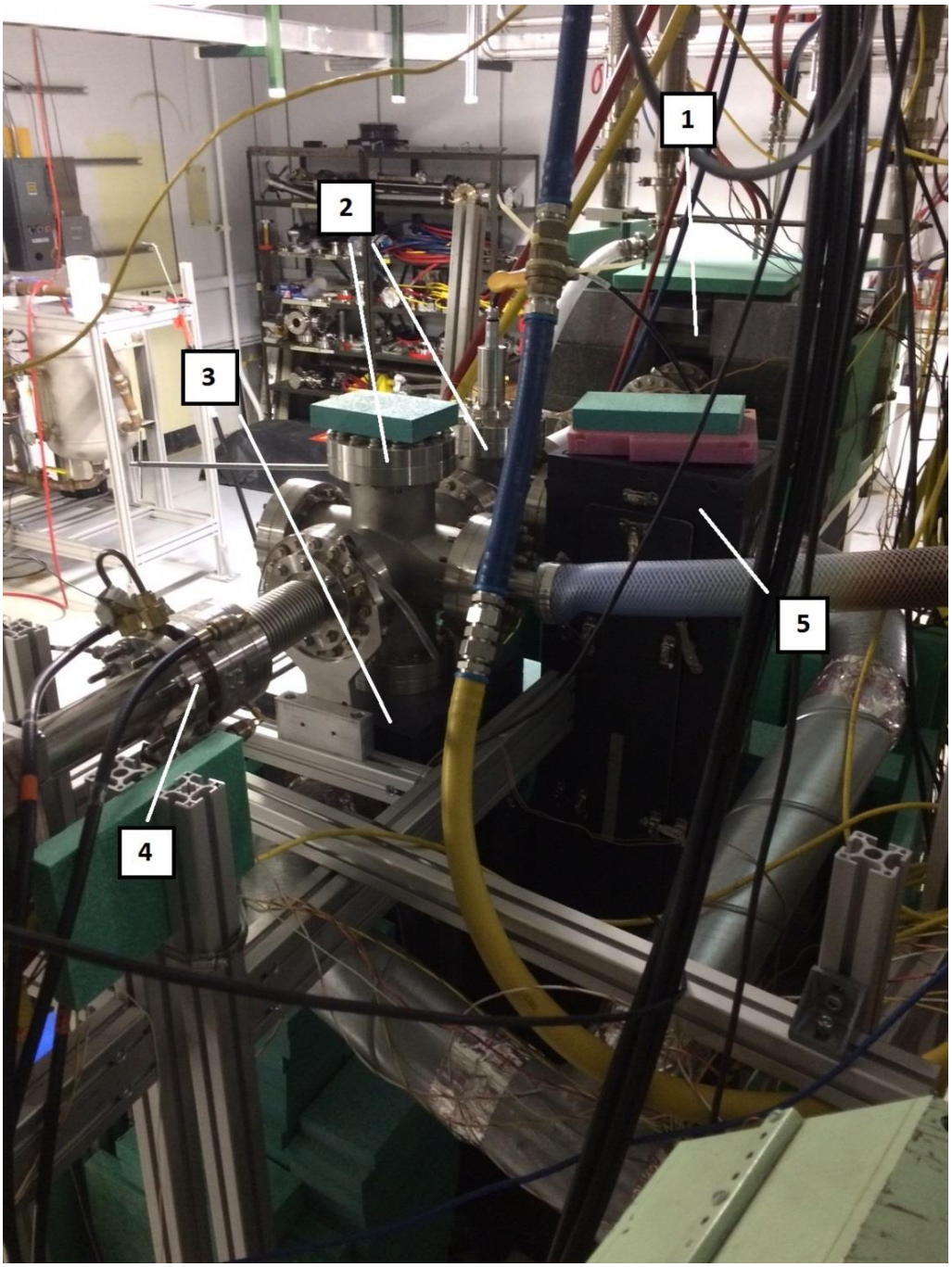

Figure 1. Beamline Used in Thermal Test
1 – NorthStar target station; 2 – six-way crosses with mirrors; 3 – Enclosure with IR camera; 4 – BCM and BPM, 5 – Enclosure with OTR-camera.

Cooling System Description, Testing, and Analysis

The helium-cooling system is connected to the inlet and outlet of the target. It provides helium gas flow at high pressure through the target disks to keep the temperature within the safe range. In this experiment, the helium pressure in the system varied from 160 to 285 psig.

Field tests were performed and the results used to validate the thermal hydraulic computer analyses for both the overall helium cooling system and the target assembly. The purpose of this work was to provide reliable computer models that could be used in evaluating the thermal analysis of the beam window. Both the 29mm and 12mm window target assemblies were evaluated.

The helium cooling system diagram is shown in Figure 2 The vessel maintains the static pressure in the system. A motor and blower are located inside the vessel and are used to circulate the flow through the closed system. An after cooler heat exchanger is located outside the vessel at the discharge of the blower. This removes the heat from compression and from the motor. A filter is located downstream of the after cooler and upstream of the target assembly to prevent particle blockage in the target coolant channels. There is a bypass around the target assembly for system recirculation when the target is not in place. The target assembly is shown below and is described later in detail. A heat exchanger located in the return from the target removes the heat generated in the target. The flow is returned to the vessel at the discharge from the heat exchanger.

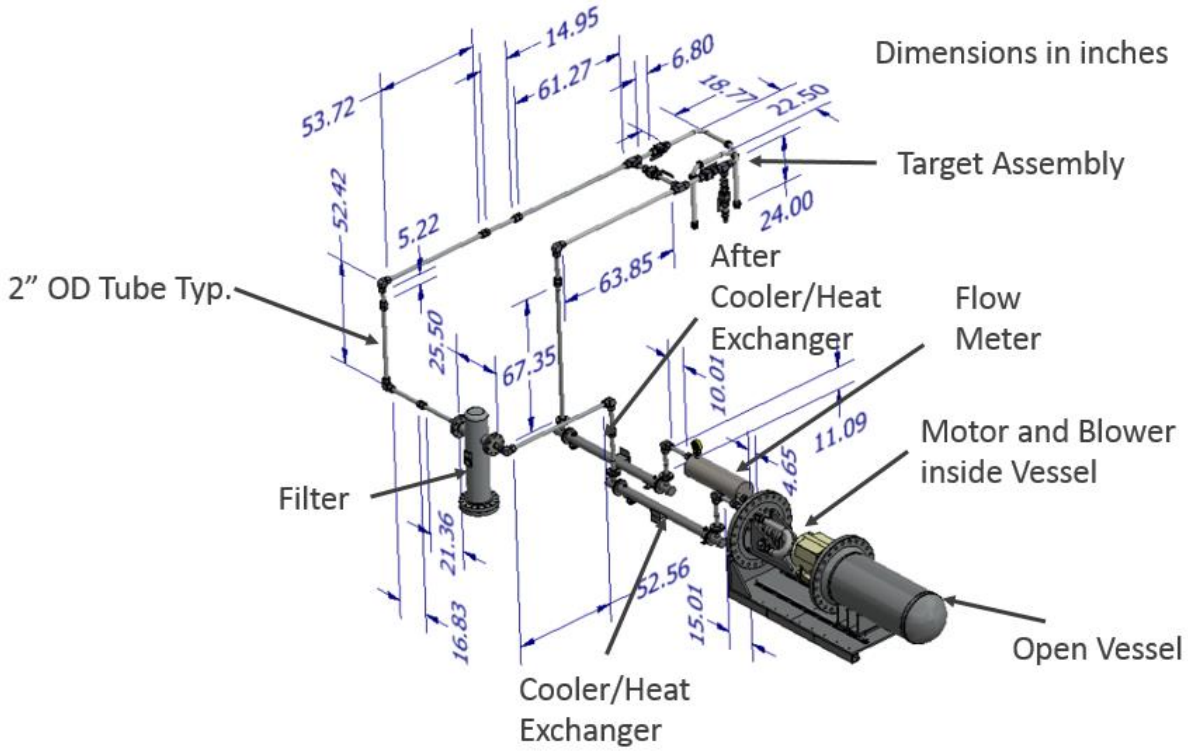

Figure 2. Helium Cooling System Diagram

The AFT Arrow computer model shown in Figure 3 was used for the thermal hydraulic analysis of the 29mm target assembly.[7] AFT Arrow is a verified/validated commercial computer code for analysis of compressible flow in piping systems.

Pressure and temperatures in the helium reservoir vessel (PT100 and TC100) were field-measured during the test and their values (270psig & 31°C) input into the computer model along with the measured mass flow (92g/s). The tubing sizes, lengths, and fitting were modeled as shown. The pressure and temperature (PT101 & TC101) out of the blower were calculated by the code (294psig & 53°C) and are in agreement with the test results. The flow resistances (K=30) through the coolers were adjusted to be in agreement with field measurements. These resistances were found to be in agreement with typical tube and shell exchangers' flow resistances. The heat removal through the after cooler (-4.3kW) was calculated considering an enthalpy balance in the helium flow across the cooler. This heat removal rate is also in agreement with typical heat exchangers. Temperature of the helium flow into the target assembly (TC102) is in agreement with measurement (23°C). The calculated pressure at the inlet to the target assembly (PT102) is not in good agreement with measurement (292psig compared to the measurement of 301psig). Noting that the creditable pressure value at the blower discharge (294psig) is significantly below the measured pressure downstream indicates that the downstream pressure value is suspect due to a transducer failure in the high radiation environment and, therefore, is assumed in significant error. The calculated pressure value (292psig) is reasonable and is assumed correct. The pressure differential across the target (DP101) and heat loss (-2kW) are to be compared to that calculated in the CFX modelling to follow. The calculated He temperature at the outlet to the target assembly (TC103) is in agreement with measurement (27°C).

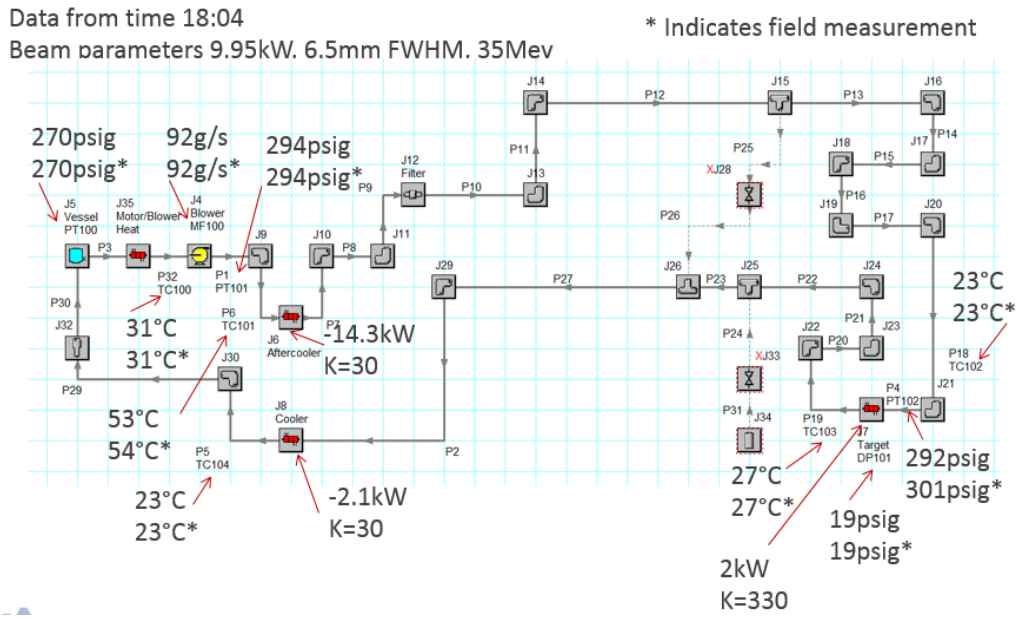

Figure 3. Computer Model and Results for the 29mm Target Assembly Cooling System

Lastly, the heat loss through the cooler (-2.1kW) and flow resistance (K=30) are within the expected performance of a tube and shell heat exchanger. The helium return temperature (TC104) to the vessel is also in agreement with measurement.

Similar helium cooling system analysis was performed for the 12mm target assembly. The model and results are shown in Figure 4. Results for this analysis were similar to those of the 29mm target assembly.

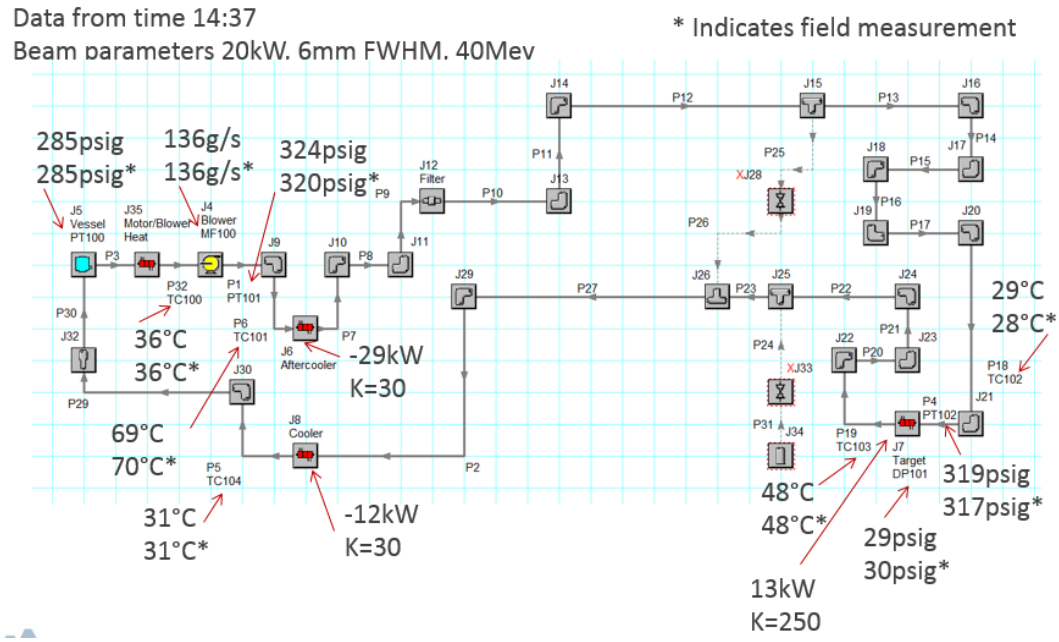

Figure 4. Computer Model and Results for the 12mm Target Assembly Cooling System

Figure 5 shows the general overall target assembly arrangement for both the 12mm and 29 mm targets. The target holder contains the disks with flow channels between each disk. The holder is inserted into the target housing that provides the pressure boundary for the helium coolant. The beam window is integral with the housing and is shaped to minimize beam attenuation and still provide adequate containment of the pressurized helium. Helium flow is directed into the target holder from the cooling system and then returned to the system.

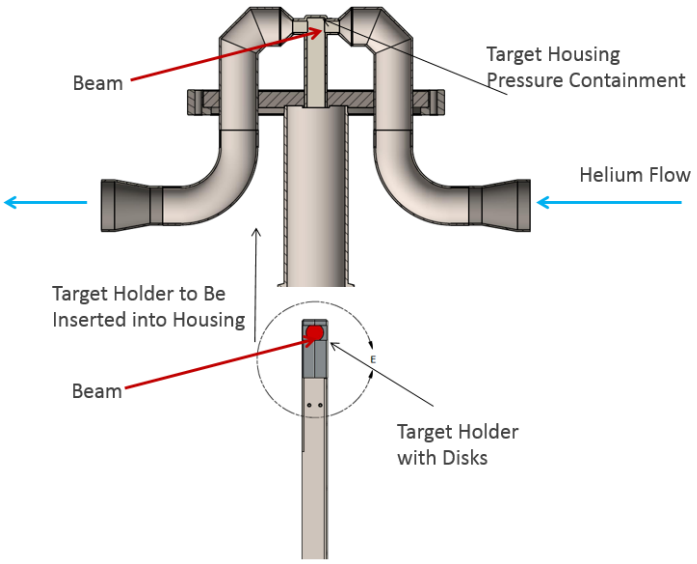

Figure 5. General Overall Target Assembly Arrangement

12 mm Target Description

Figure 6 shows the detailed design of the 12mm target assembly. This assembly was designed by LANL and previously described in [1, 2]. The holder contains 25 molybdenum disks that are 12mm (0.47in) in diameter and 1 mm thin with 26x1 mm flow channels. The beam window is integrated with the Inconel housing with dimensions as shown.

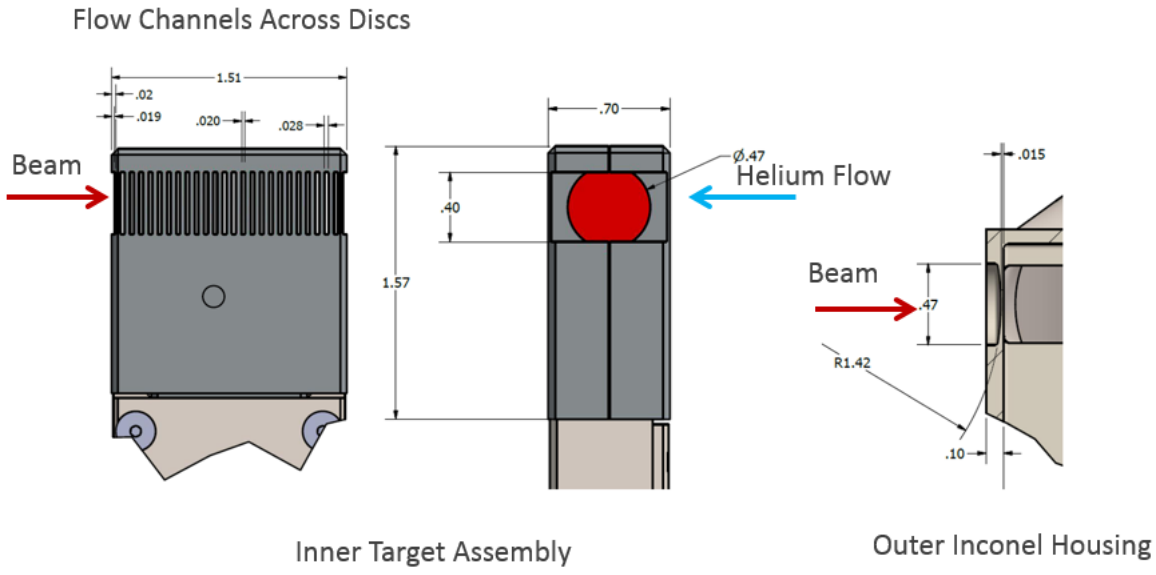

Figure 6. 12mm Target Design

29 mm Target Description

Figure 7 shows the detailed design of the 29mm target assembly. The holder contains 10 molybdenum disks, each 29mm (1.14in) in diameter but having different thicknesses with 11 flow channels. The beam window is integral with the Inconel housing with dimensions as shown.

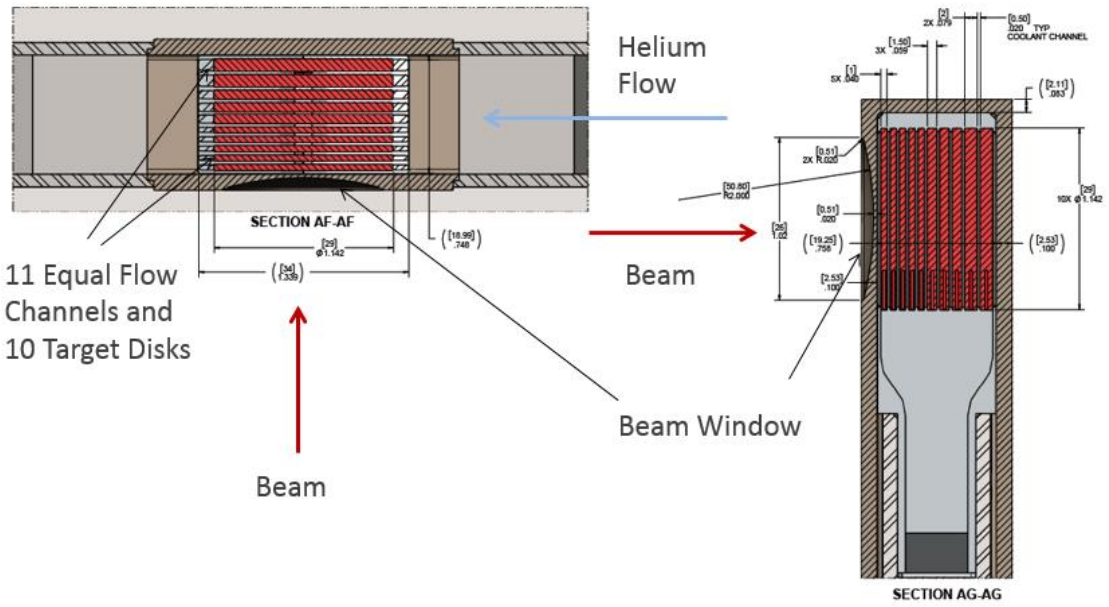

Figure 7. 29mm Target Design

Instrumentation

Optical Transition Radiation (OTR) Camera

In our experiment optical transitional radiation is produced by relativistic electrons when they cross the interface between vacuum and window material. Because most of the transition radiation falls in the visible range, an ordinary monochromatic camera is used to monitor beam size and position at the target window. A Basler™acA640-120gm GigE camera with Sony ICX618 CCD is used. The camera generates a black-and-white picture with resolution of 659x494 pixels with a repetition rate up to 120 Hz. The camera trigger is synchronized with the beam. The camera is installed in a plastic box at a distance of 1.5 meters from the target window and positioned at the target face through two mirrors. The box is shielded by lead bricks for X-ray protection and by borated poly bricks for neutron protection.

The team developed the OTR-camera software controls and camera parameters in-house and acquired the images (Fig. 8). After the camera is installed in the box, the target is illuminated by the LED light. The calibration factor is set using target window transverse size as a reference. The beam's image is processed according to data gathered from two areas: horizontal and vertical beam intensity histograms. These data are analyzed by GSL scientific numerical library code (www.gnu.org/software/gsl) to approximate it by the RMS algorithm for Gaussian envelope. The calculated beam transverse is sized at Full Width at Half Maximum (FWHM) and its position is transferred to an EPICS-based Linac control system. These numbers are used in the machine interlock to stop irradiation in case of beam abnormal size of position at the target to protect the target holder from damage. The periodical logging of the picture is used for image post-processing.

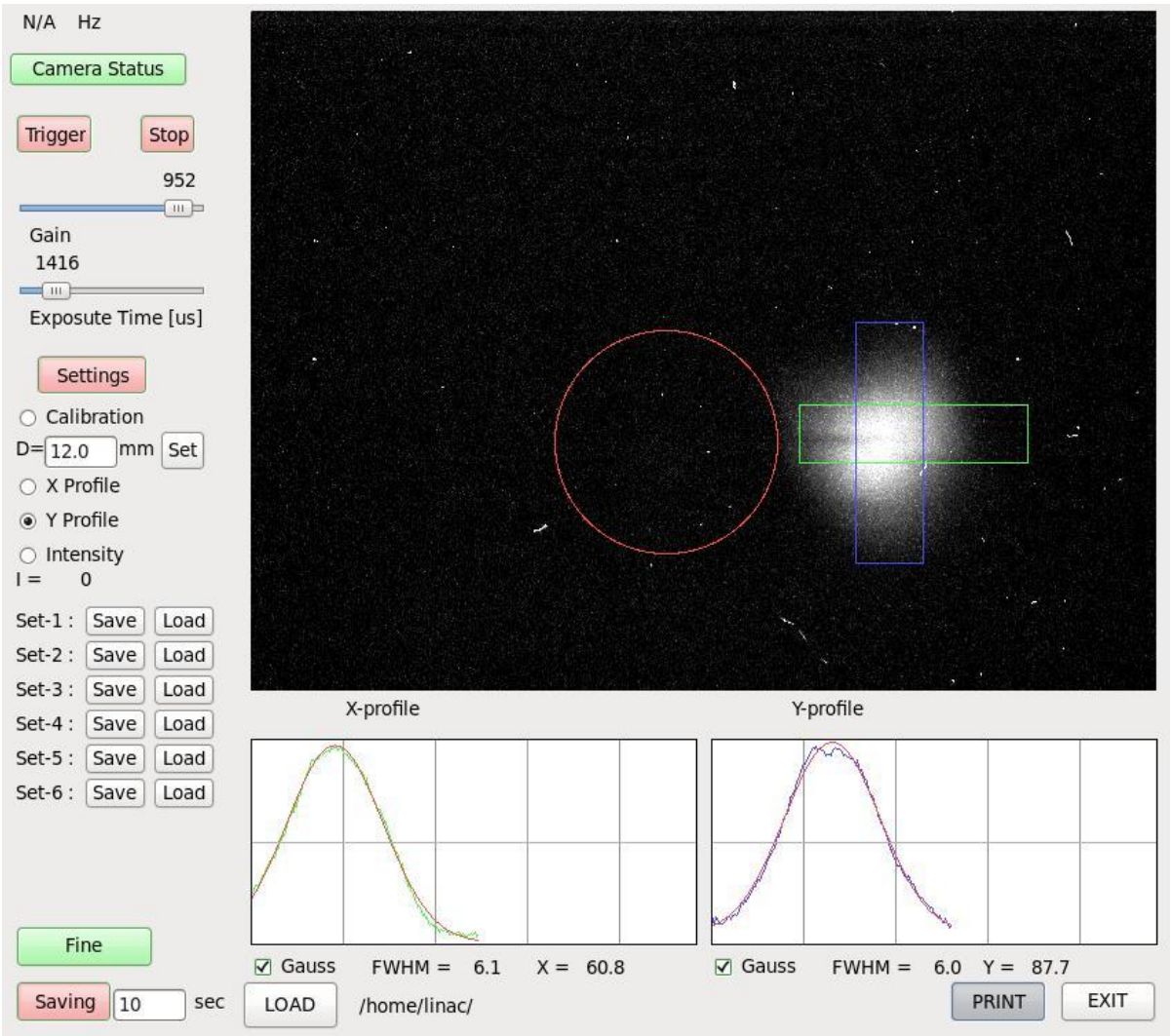

Figure 8. Screenshot of saved image captured with OTR-camera with beam profile and position at the target.

Flir™ Infra-Red Camera

To measure the window surface temperature, a FLIR A655sc Infra-Red thermal imaging camera (IR camera) with an 89mm lens was installed 2.5 meters from the Inconel window. It was shielded by the LED bricks and borated polyethylene sheets, and centered at the target face by one mirror. The measurement of surface temperatures is highly dependent on the emissivity of the window surface and transmission parameters of the elements in the optical path. These parameters were determined at Los Alamos previously by using an identical window. The surface emissivity estimation was 0.422 and transmission of the optical camera path was 0.372. These parameters were used in the FLIR ExaminIR camera control software for all thermal tests.

IR Camera Calibration

The IR-camera calibration was verified before each irradiation. The heater (Fig.10) was installed in the target place and the temperature measured by thermocouples and IR camera. The IR-camera response, measured in two points to the heater temperature, is linear (Fig. 9). The measured temperature is periodically logged to the computer for post-experimental evaluation.

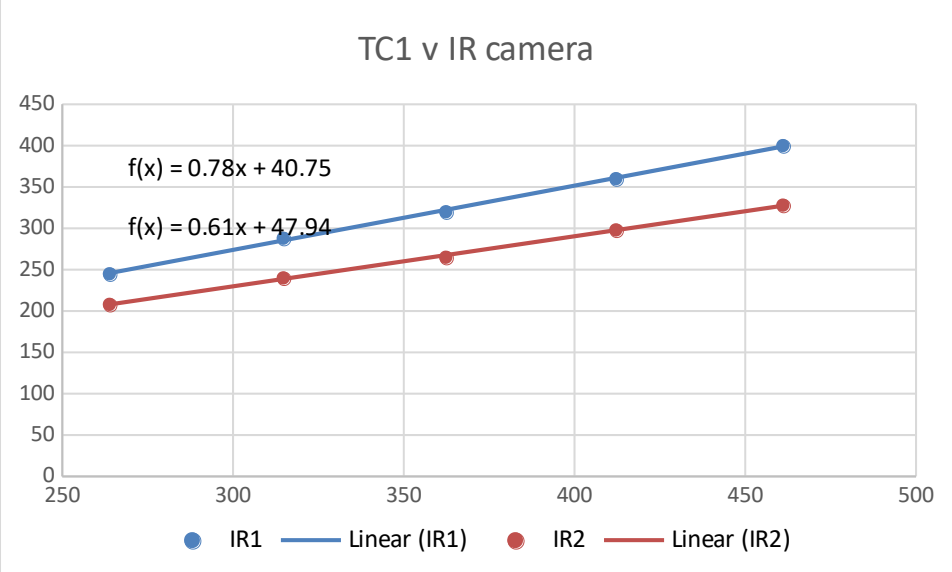

Figure 9. Linearity of IR-camera measurement on two points vs heater temperature.

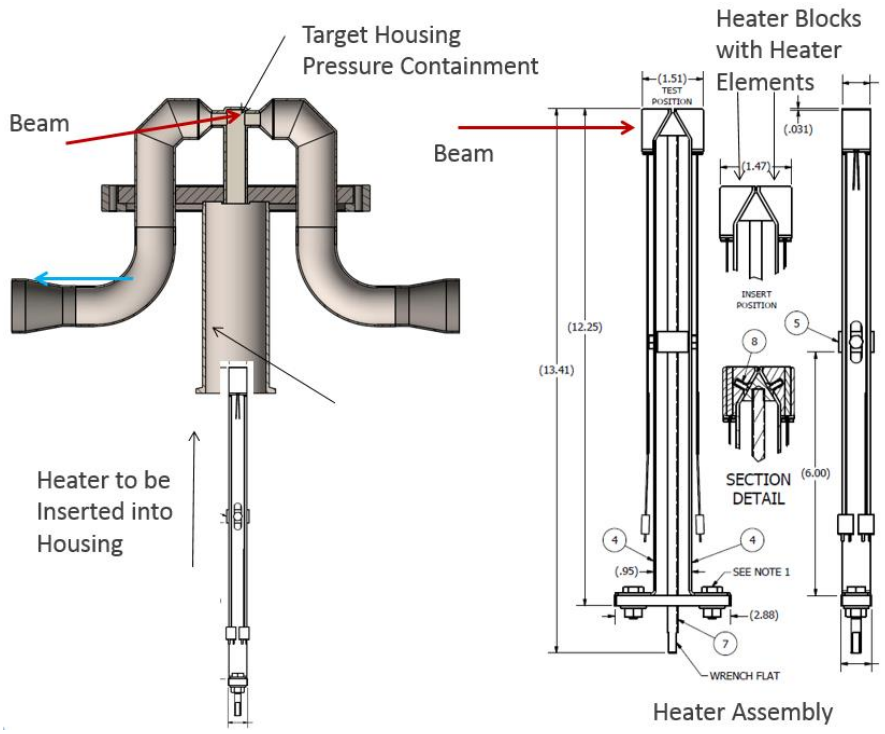

Figure 10. Window heater design for IR camera calibration.

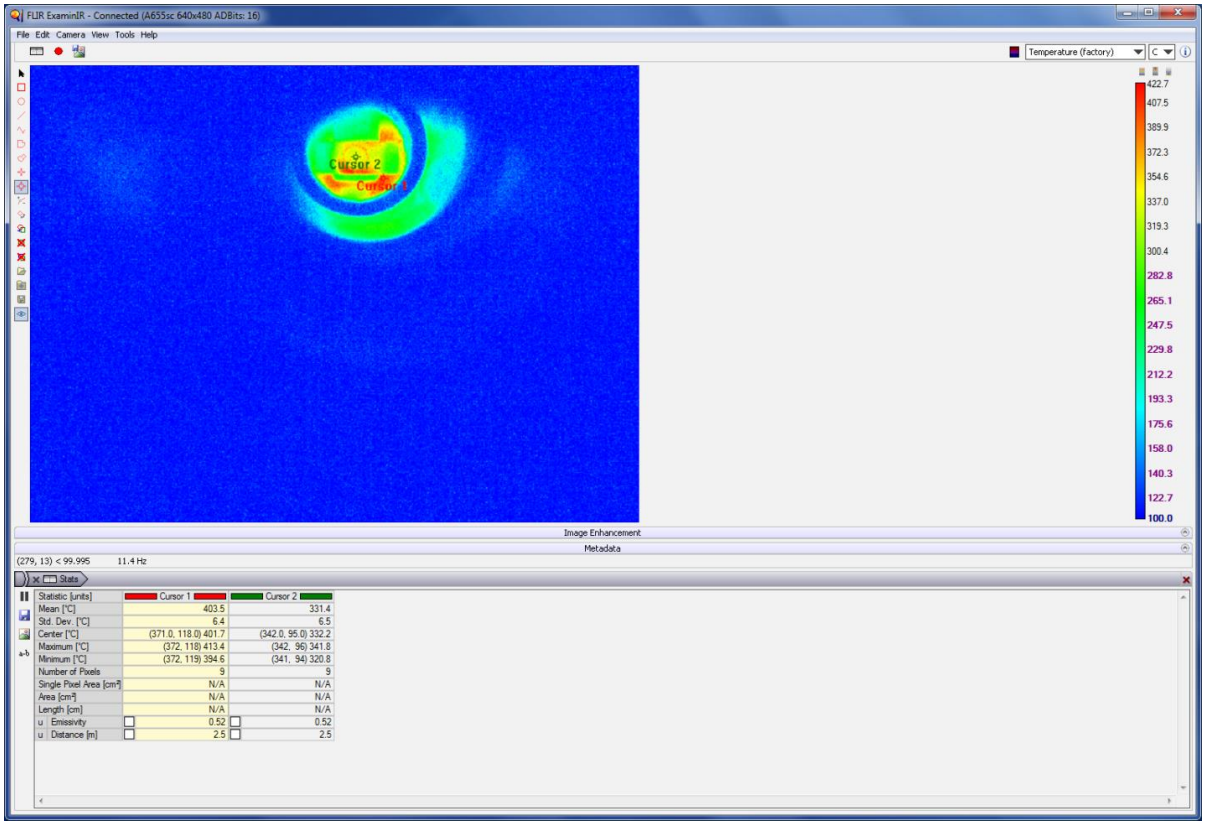

Figure 11. IR-camera monitoring of window temperature.

Beam Current Monitors

Beam current monitors (BCMs) are used for continuously monitoring the beam current during irradiation. BCMs are based on a BERGOZ™ Fast Current Transformer FCT-CF4.5”-34.9-UHV-1.25-LD-H with rising time no worse than 1nS. The output signal is a current to be measured across a 50 Ohm load. Radiation resistance of all BCM components are $>10^6$ Gy.

BCMs are installed in the beamline at the exit of the acceleration portion of the machine, transport channel, and before the target. We used BCM measurements to control the beam pulse current, average current, and average beam power at the target. Average beam power is calculated “on-the-fly” based on beam actual current, beam energy, and repetition rate. The data is periodically logged into a separate file on the monitoring computer.

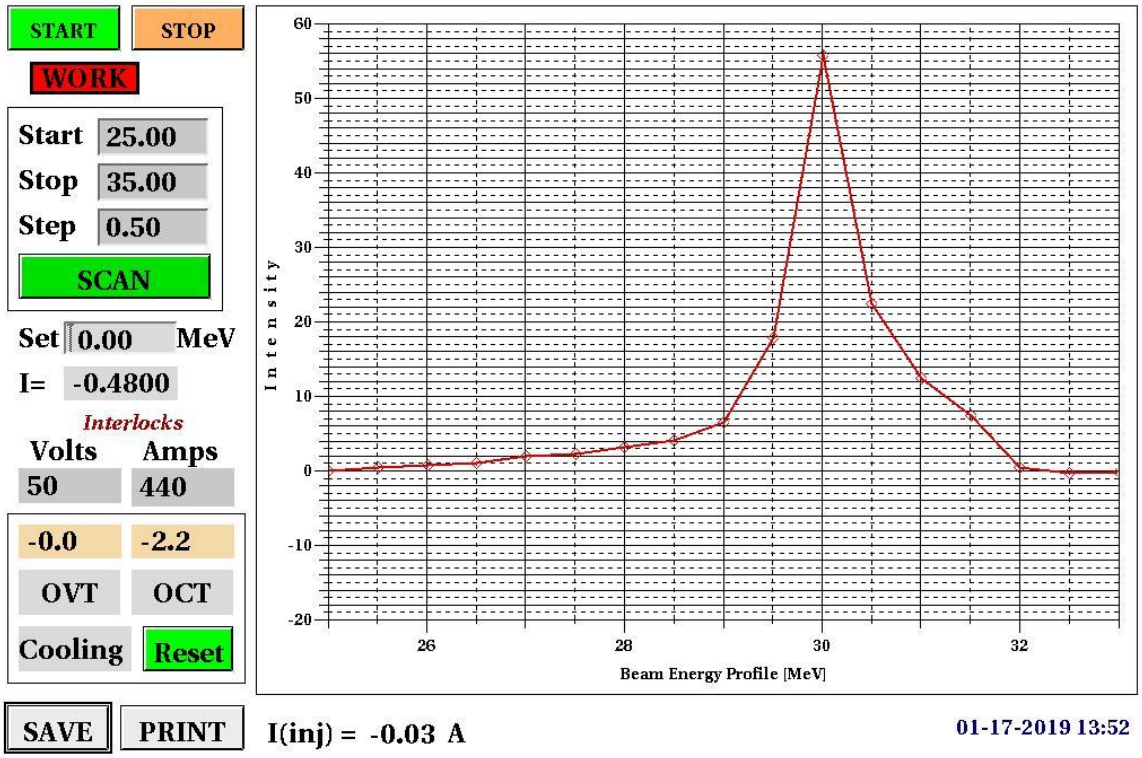

Figure 12. 30 MeV Beam Energy Spectrum

29mm Target Window Experimental Data

For experiments with a 29-millimeter target, the beam energy was tuned up to 30 MeV. A typical beam energy spectrum is shown in Figure 12. The beam pulse current was -0.86A, and beam size at the target window was -6.5x6.5 mm. Two full runs were performed with two different pressures in the helium cooling system: 200psi and 285psi. The maximum power was 10 kW (Figure 13); it was restricted by the temperature of the thermocouples installed at the target disks (Figure 14). The power of the beam was changed in steps with values 1.6, 3.2, 6.4, and 10 kW of the beam average power. Three stepped runs were performed for each helium pressure.

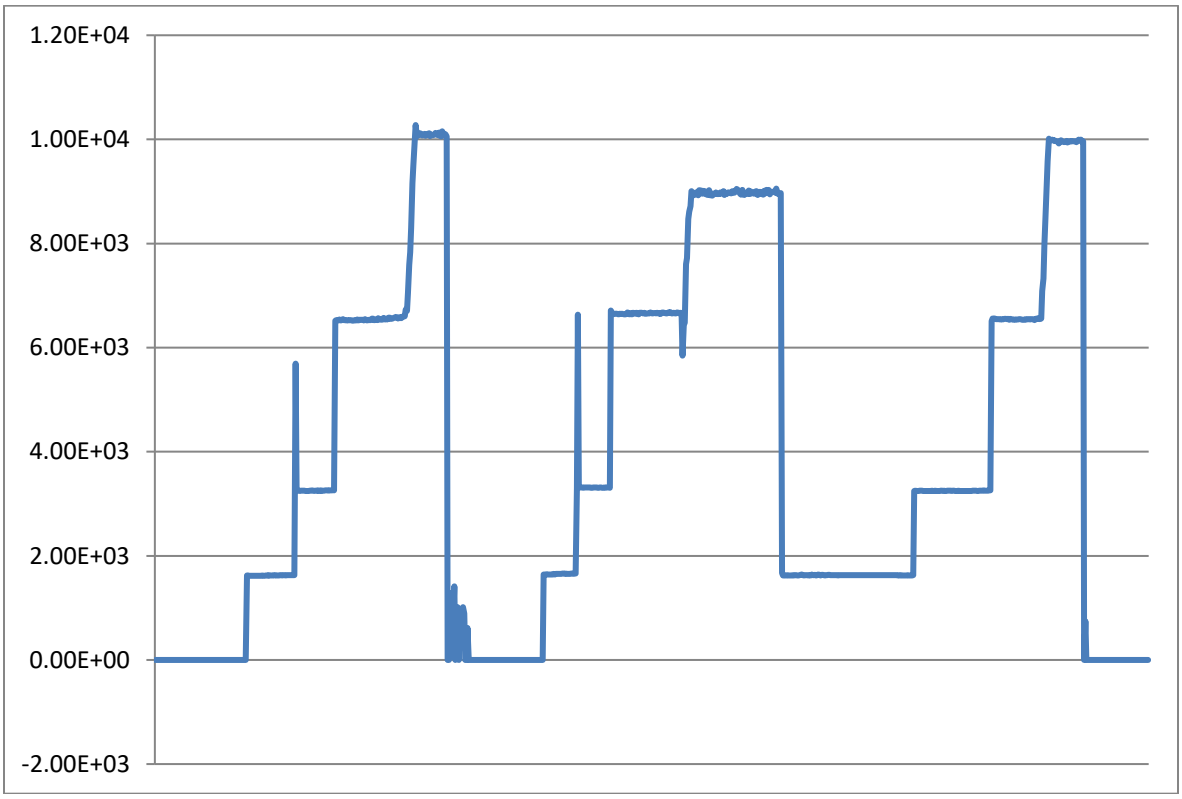

Figure 13. Average Beam Power [W] History Sample from BCM Data

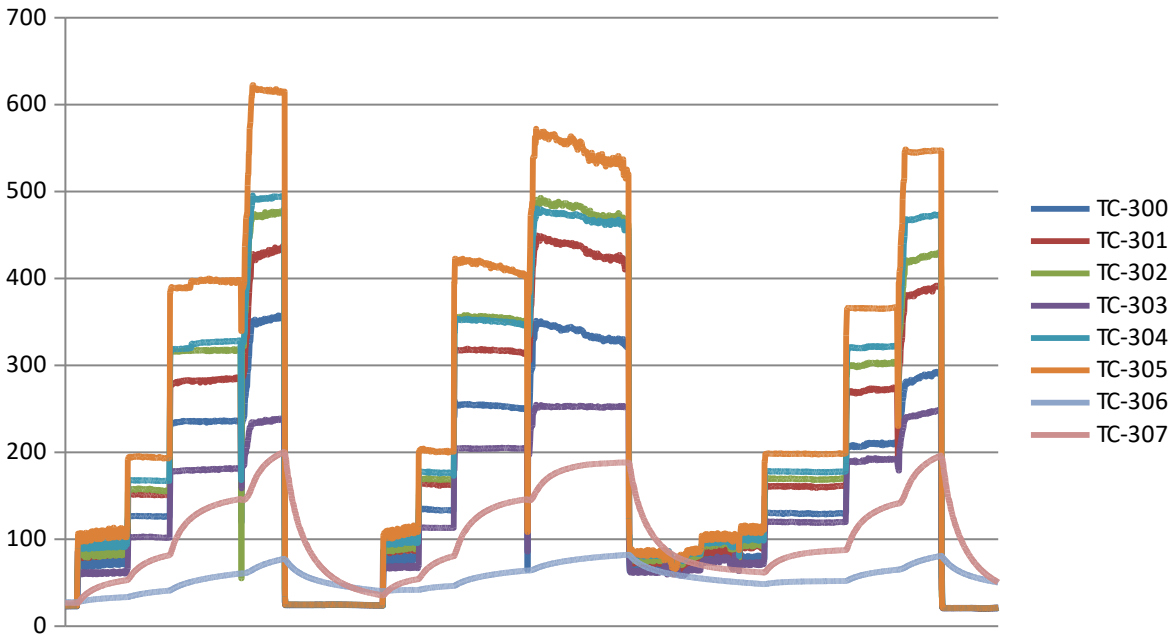

Figure 14. Thermocouples Readings at Different Beam Powers at Helium Pressure 285 psig

The ultimate beam power was restricted by the temperature of the target. The maximum value could not exceed 640C.

Temperature was measured by IR camera looking at the target window and thermocouples installed at the first six disks of the target. Due to the changes of thermal load on accelerator structures with rising of repetition rate, the beam energy changes slightly, which led to variation in the beam size at the target window. Measurements of the beam vertical and horizontal sizes are presented in Tables 1a and 1b.

Table 1a. Window Temperature and Beam Size for Helium Pressure 200 psig

		Beam Size, FWHM [mm]	
Power [kW]	Window Temperature	X	Y
1.6	120	6.6	6.5
3.2	210	6.4	6.6
6.4	375	6.4	5.7
10	540	5.2	4.0
1.6	110	6.6	6.6
3.2	210	6.4	6.4
6.5	415	5.6	4.8
10	570	No data	

Table 1b. Window Temperature and Beam Size for Helium Pressure 285 psig

		Beam Size, FWHM [mm]	
Power [kW]	Window Temperature	X	Y
1.6	<100	6.8	6.4
3.2	150	6.8	6.3
6.5	300	5.5	4.5
10	440	4.9	3.4
1.6	<100	4.8	3.6
3.3	160	6.8	6.1
6.5	320	5.2	4.3
9	420	5.8	5.0
3.2	240	9.1	9.3
6.5	260	10.2	9.5
10	380	11.8	8.5

Helium Cooling System

The helium cooling system is designed to provide a cooling process for the molybdenum disks and target windows during irradiation. The helium pressure ranges to 285 psi, with a mass flow rate of up to 136 g/s. The closed gas loop goes through the heat exchanger and cooled down to 27°C. The heat removal after cooler is presented in the Table 2.

Table 2. Heat Removal [W] from 12mm Target for Different Average Beam Power

Beam Power [kW]	158 psi	205 psi	285 psi
5.2	2543	3388	2649
10	4860	5560	4957
16	7119	7564	7833
20	N/A	N/A	9234

12mm Target Window Experimental Data

The thermal test with the 12mm window was performed with beam energy of 40 MeV and an initial beam size of 6.0x6.1 mm. The irradiation was performed for three helium gas pressure values: 160psi, 205psi, and 285psi. The beam size at the target window did not change during the run.

Unfortunately, the first thermal test with this window, begun on April 25, 2019, had to be stopped when the temperature of the water-cooled beam dump rose above desired values. Irradiation was halted and a new cooling water line with greater water flow was connected to the beam stop. The next experiment was performed on May 2, 2019.

Because thermocouples were not installed at this target, target temperature measurements were not available. Window temperatures were obtained from IR-camera images of the target window. The table of measured windows temperatures versus beam power and Helium pressure is presented in Table 3. Also, a plot of these temperatures is shown in Figure 15.

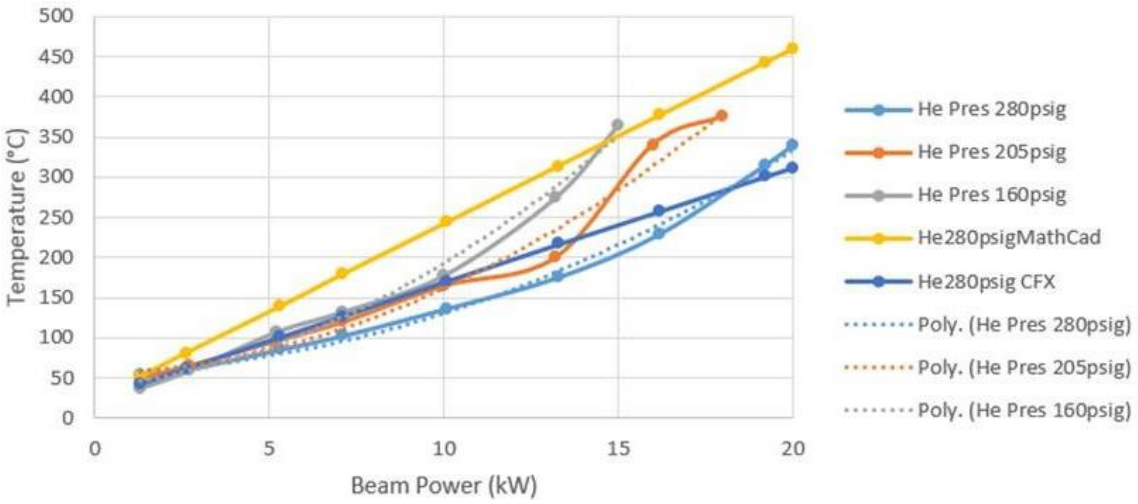

Figure 15. Peak Window Temperature vs Beam Power for 6mm FWHM Beam

Table 3. Target Window Temperature as a Function of Beam Power at Three Helium Pressures

	Window Temperature		
Power [kW]	160 psig	205 psig	280 psig
1.3	38	51	55
2.7	60	66	61
5.2	108	97	86
7.1	133	120	103
10.0	178	165	137
13.2	275	200	176
15.0	365		
16		340	230
18		375	
19.2			315
20			340

Computation Flow Dynamic (CFD)Analysis 29mm Diameter Target Assembly

ANSYS CFX is used to evaluate the hydraulic performance of the 29mm diameter target assembly.[8] The model assumes that the flow through the target is equally distributed among the eleven channels and, therefore, a single channel analysis is considered sufficient.

Figures 16 and 17 show the results of the analysis. The assumed boundary conditions are shown on the velocity vector plot along with the assumed geometry. Symmetry boundaries are used to simulate the entire inlet and outlet plenums. The target disk surfaces are modeled as "no slip" walls. Mass flow rate is determined by considering the total flow rate (92g/s) and dividing by 11. The outlet is held at a uniform static pressure of 270psi. Velocity results are consistent with hand calculations and are later used to determine the thermal convective coefficient.

Figure 17 displays the pressure contour results. The indicated pressure differential from inlet to outlet is approximately 6psi. This is in reasonable agreement with classical correlations as shown there (5.82psi). However, this pressure differential is considerably lower than was field-measured, as indicated in the earlier system analysis. This will be addressed in the conclusion.

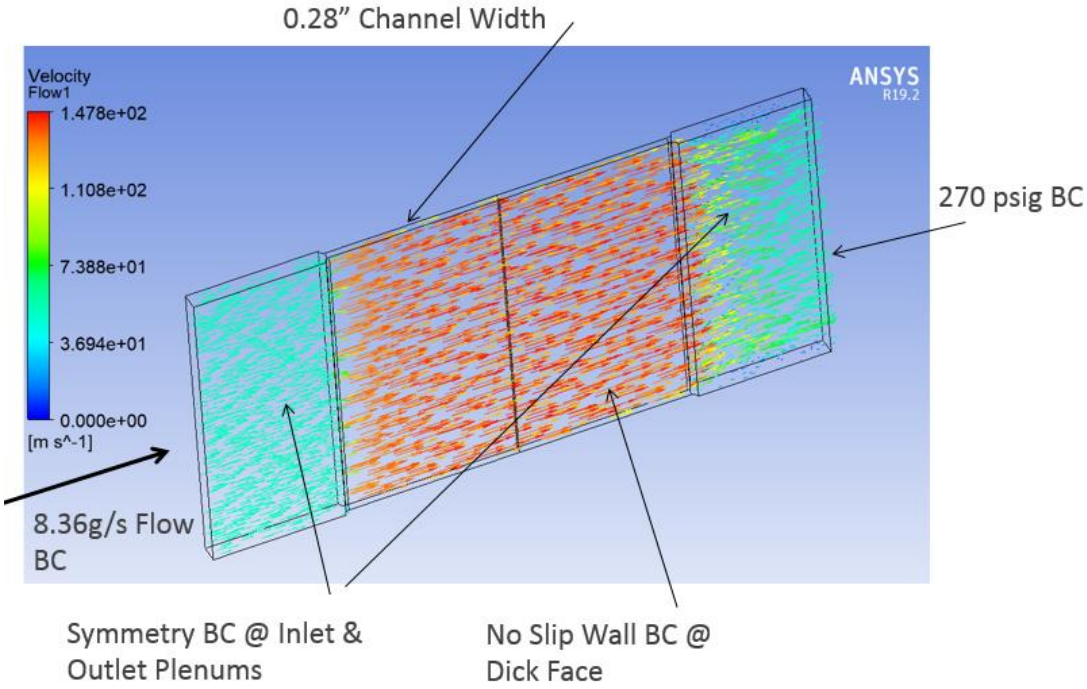

Figure 16. ANSY CFX Hydraulic Analysis of Flow Across Target Disks, Velocity Vectors

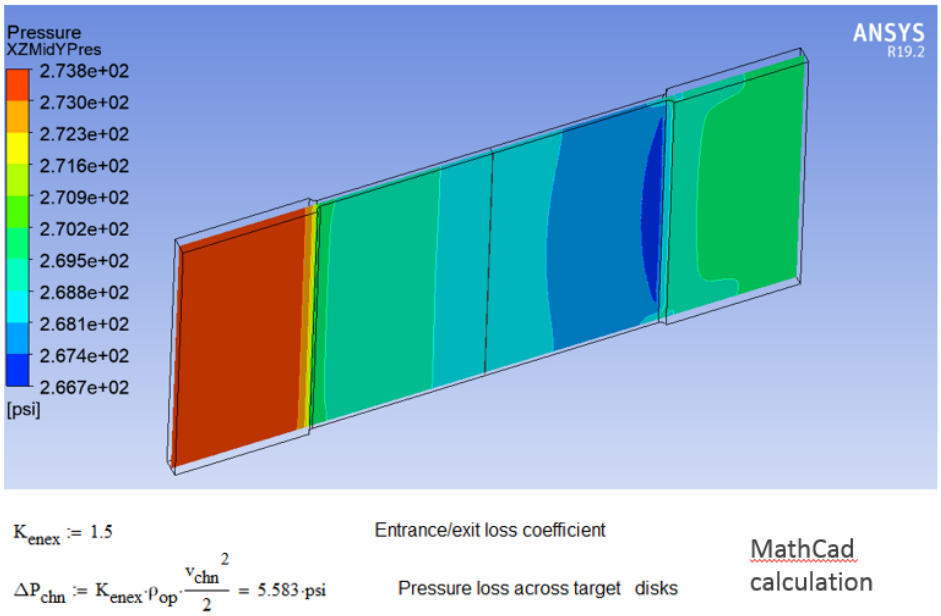

Figure 17. ANSY CFX Hydraulic Analysis of Flow Across Target Disks, Pressure Contour

ANSYS CFX is used to evaluate the thermal hydraulic performance of the target assembly beam window. The model assumes that since the flow through the target is equally distributed among the eleven channels, a single channel analysis is considered sufficient. Therefore, the analysis considers the singular flow channel at the window. A symmetric half-model is used to simplify the modeling.

Figures 18, 19, and 20 show the results of the analysis. The assumed boundary conditions are shown on the velocity vector plot along with the assumed geometry; with the exception of the boundary conditions, they are not noted and are defaulted to adiabatic. The symmetry boundary condition is used to create a simpler half-model. Because heat from the first adjacent disk is assumed negligible, the outer wall B.C. is modeled as adiabatic. The target window surface of the channel is modeled as a “no slip” wall with heat transfer. Mass flow rate is determined by considering the total flow rate (92g/s) and dividing by 11. From this value and the cross-sectional area of the channel, the average flow velocity (126m/s) is calculated and input to the model. The outlet is held at a uniform static pressure of 270psi. Velocity results are consistent with hand calculations and are later used to determine the thermal convective coefficient.

The temperature contour results shown in figures 19 and 20 indicate a maximum temperature of 629°C, which occurs at the beam center on the beam side of the window. This temperature was field-measured using an IR camera and recorded a temperature of approximately 500°C at the given beam conditions. There is a 25% difference between the measured and CFX temperatures. This significant difference will be addressed in the conclusions. Also, a hand calculation using classical correlations indicated a window temperature of 543°C at the outer window surface. This value is in reasonable agreement with measurement.

Lastly, Figure 20 shows the temperature gradient through the thickness of the window at the center, displaying a large gradient of 65° from outside to inside surfaces. This gradient is in reasonable agreement with hand calculations.

CFX Results Compared to Field Measurements

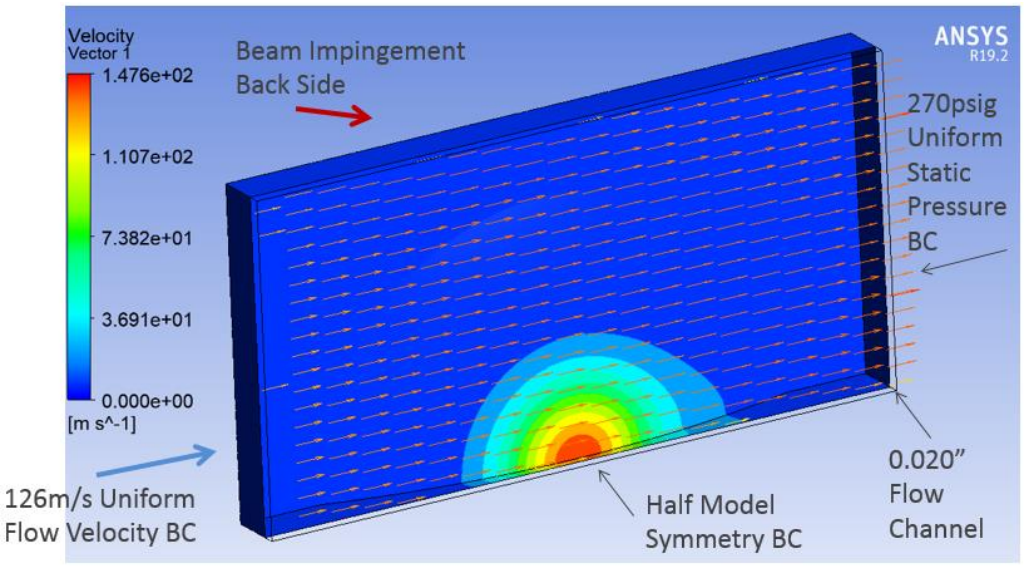

Figure 18. ANSY CFX Thermal Hydraulic Analysis of Window at Beam Parameters: 9.94kW, 6mm FWHM, 35Mev Velocity Flow Vectors

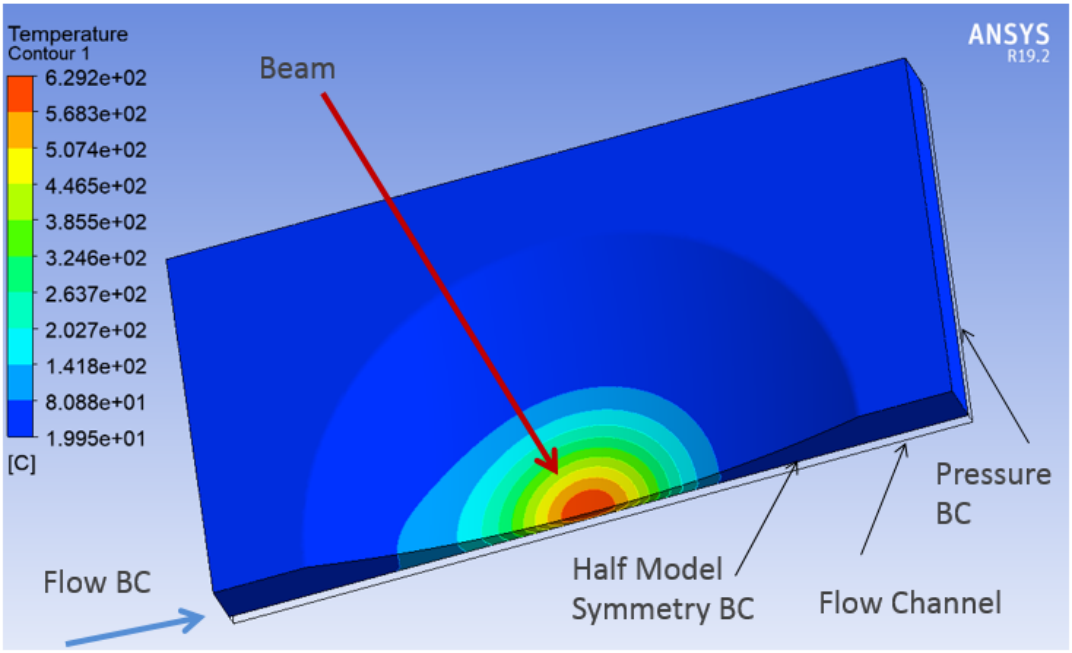

Figure 19. ANSY CFX Thermal Hydraulic Analysis of Window at Beam Parameters: 9.94kW, 6mm FWHM, 35Mev Temperature Contours Surface

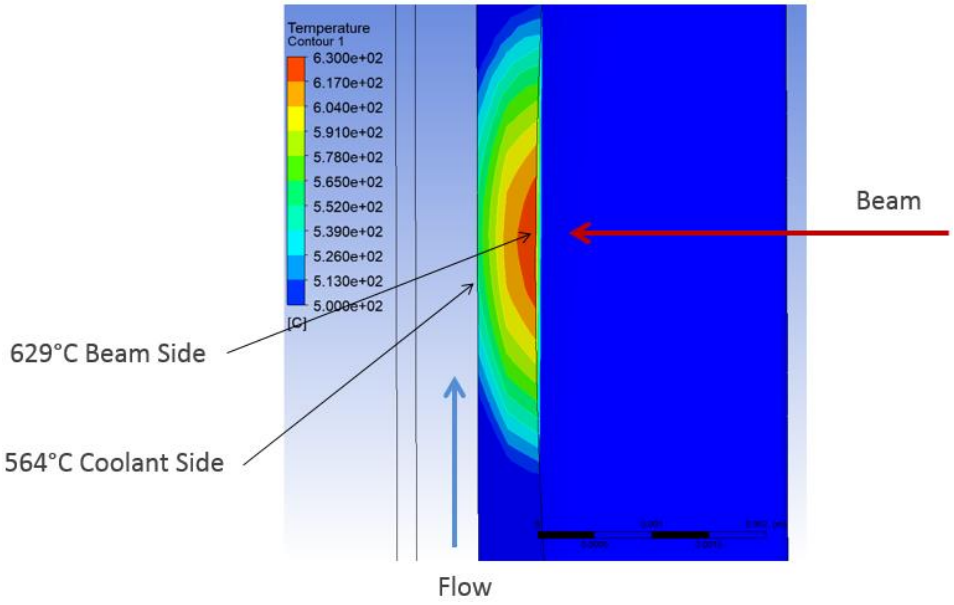

Figure 20. ANSY CFX Thermal Hydraulic Analysis of Window at Beam Parameters: 9.94kW, 6mm FWHM, 35Mev Temperature Contours Section Through Center

CFD Analysis 12mm Diameter Target Assembly

ANSYS CFX is used to evaluate the thermal hydraulic performance of the 12mm diameter target assembly.[8] Because the model assumes that the flow through the target is equally distributed among the 26 channels, a single channel analysis is considered sufficient.

The CFX model geometry is shown in Figure 21. The curved beam window is integral with the Inconel housing. The helium flow channel is modeled as a rectangular slot in the housing. A tantalum half-symmetric disk is modeled at the back side from the beam. Dimensions are as indicated on the previous design drawings.

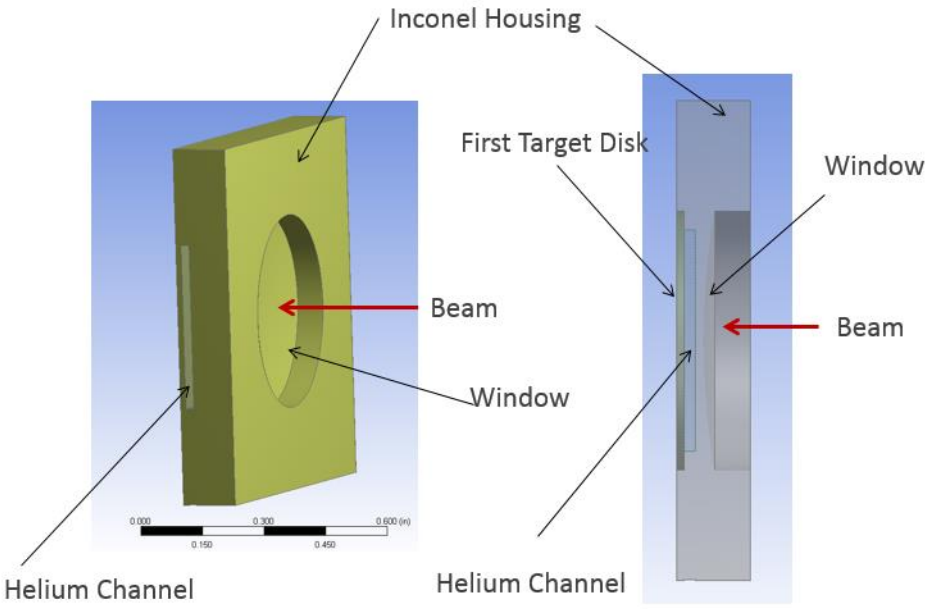

Figure 21. ANSYS CFX Geometry for the 12mm Diameter Target Window

The hydraulic results for a typical analysis case are shown in Figure 22. The assumed boundary conditions are shown on the velocity vector plot. The target disk surfaces are modeled as “no slip” walls. Mass flow rate is determined by considering the total flow rate (136g/s) and dividing by 26. The outlet is held at a uniform static pressure of 315psi. Velocity results are consistent with hand calculations and are later used to determine the thermal convective coefficient.

The pressure contour results are also shown in Figure 22. The indicated pressure differential from inlet to outlet is approximately 15psi. This is in reasonable agreement with classical correlations, as shown there (18psi). However, this pressure differential is considerably lower than the field measurement (as indicated in the earlier system analysis. This will be addressed in the conclusions.

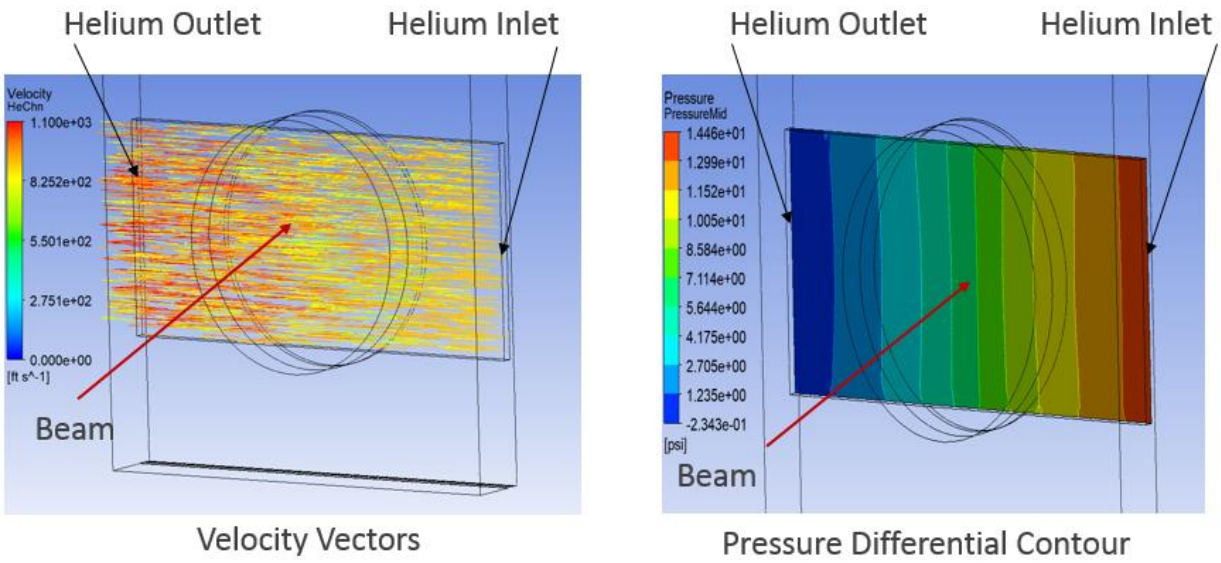

Figure 22. Velocity Vectors and Pressure Differential Contours for 12 mm Diameter Target Window

The temperature contour results in Figure 23 indicate a maximum temperature of 410°C, which occurs at the beam center on the beam side of the window. A hand calculation using classical correlations indicated a window temperature of 543°C at the outer window surface. This value is in reasonable agreement with measurement.

Figure 23 also shows the temperature gradient through the thickness of the window at the center; there is a large gradient of 46°C from the outside to inside surfaces. This gradient is consistent with hand calculations.

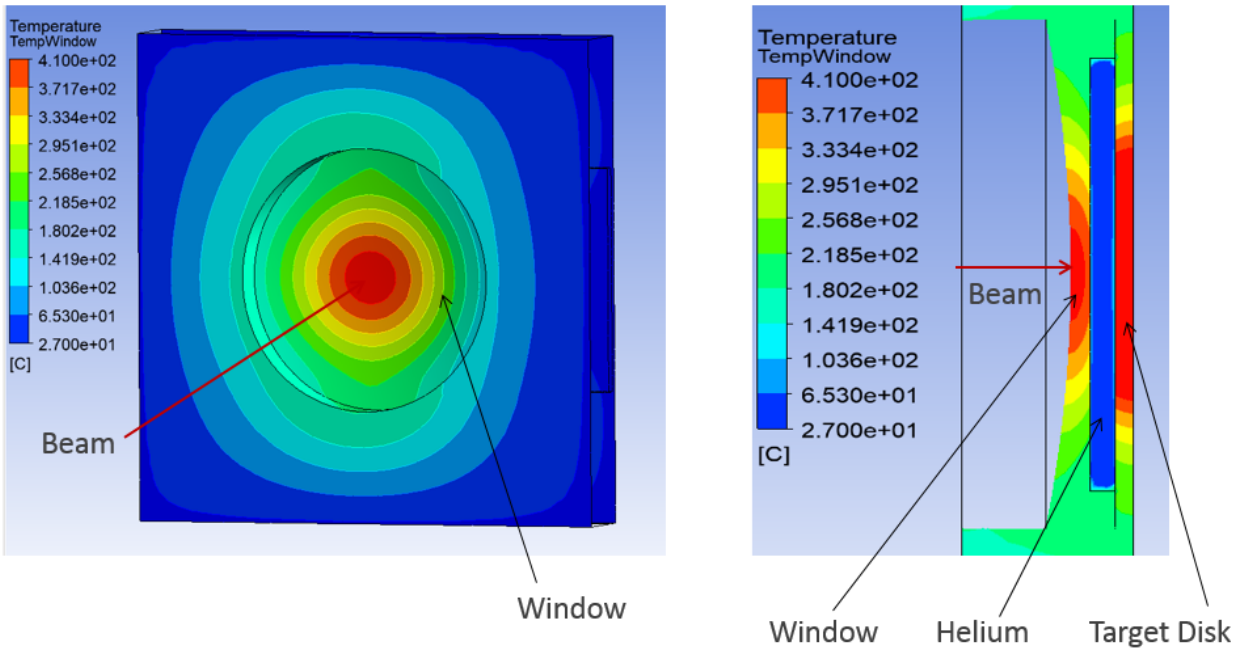

Figure 23. ANSY CFX Thermal Hydraulic Analysis of 12mm Window at Beam Parameters: 20kW, 6mm FWHM, 40Mev Temperature Contours at Front Beam Side and Section Through Center

CFX Results Compared to Field Test for the 12mm Diameter Target

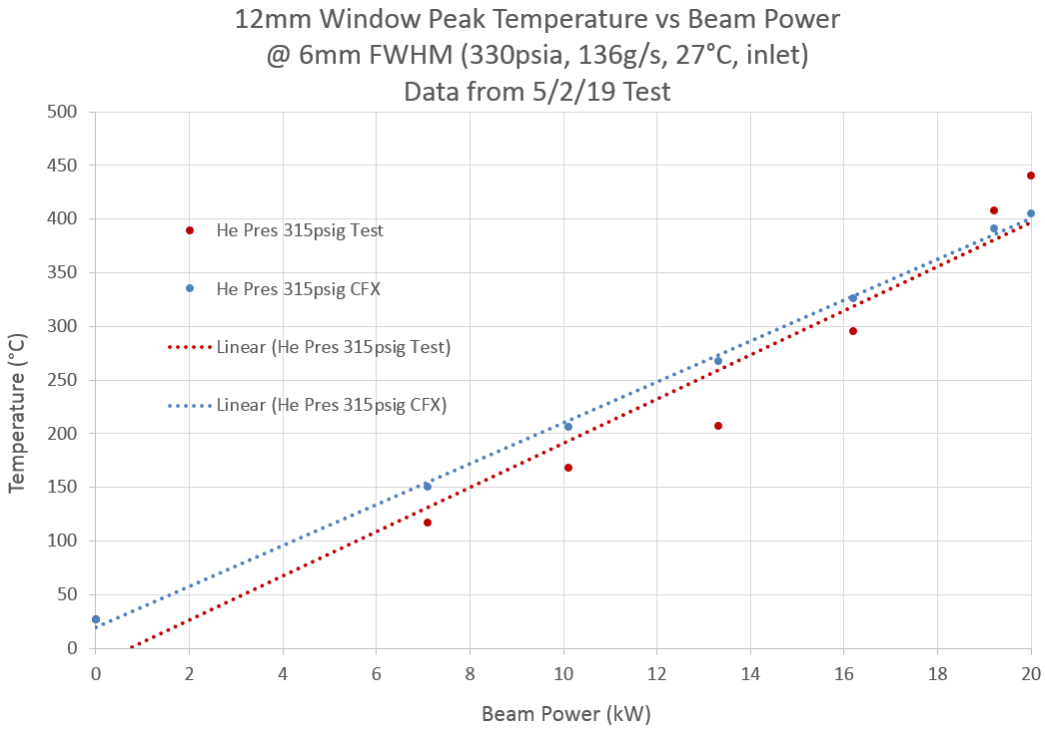

Figure 24. Measured and Calculated Window Temperatures for 12 mm Target Housing as Function of Beam Power. Helium Gas Pressure 330 psia, Flow Rate 136 g/s.

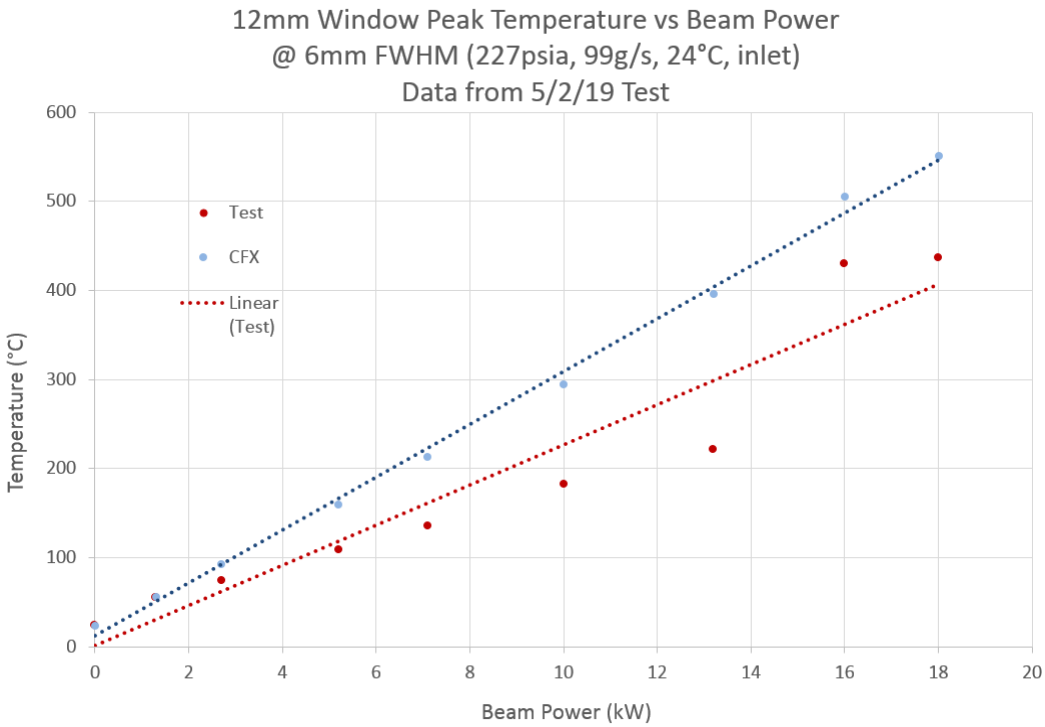

Figure 25. Measured and Calculated Window Temperatures for 12 mm Target Housing as Function of Beam Power. Helium Gas Pressure 227 psia, Flow Rate 99 g/s.

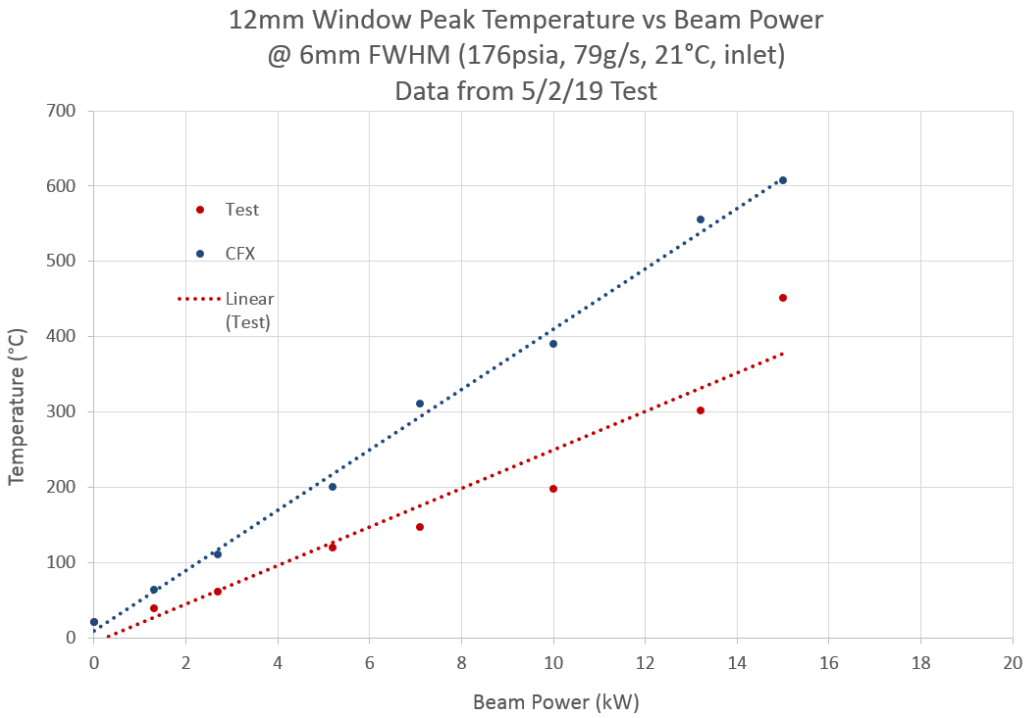

Figure 26. Measured and Calculated Window Temperatures for 12 mm Target Housing as Function of Beam Power. Helium Gas Pressure 176 psia, Flow Rate 79 g/s.

Conclusion

Helium Cooling System

Field tests and AFT Arrow computer results were in reasonable agreement. Performance of the blower, pressure losses through the system, heat exchanger capacities, and energy balances were within the expected design ranges. Note that the pressure readout from the transducer at the target inlet is in obvious error and is probably damaged from the high radiation environment.

Hydraulic Analysis of Flow Across 29mm Target Disks

The results from the CFX ANSYS for the pressure loss across the target disks 6psi is significantly different from the field measurement (19psi). It is noted that the field measurement is the pressure loss across the entire target assembly and not only across the disks as calculated. It has been assumed that the majority of the loss in the target station occurs across the disks. This assumption needs to be reconsidered and the discrepancy resolved.

Thermal Hydraulic Analysis of 29mm Window

The results from the CFX ANSYS for the maximum window temperature (629°C) is significantly different from the field-measured temperature (500°C). An IR camera was used for the field measurements and was calibrated at a maximum temperature of 400°C. A source of error to consider is that emissivity is a considerable function of temperature and thus a measurement at 500°C maybe in notable error. A preliminary evaluation of this error indicates that a maximum error due to emissivity variation is 10%. This is not large enough to account for the temperature discrepancies. Resolution of this error is needed.

References

[1] S. Chemerisov, J. Bailey, T. Heltemes, C. Jonah, R. Gromov, V. Makarashvili, P. Tkac, D. Rotsch, M. Virgo, and G. F. Vandegrift, “Results of Four One-day Electron-Accelerator Irradiations of Enriched Mo-100 Targets for the Production of Mo-99,” ANL report ANL/NE-16/26. Argonne National Laboratory (2016).

[2] S. Chemerisov, J. Bailey, T. Heltemes, C. Jonah, R. Gromov, V. Makarashvili, P. Tkac, D. Rotsch, M. Virgo, and G. F. Vandegrift, “Results of Six-and-a-Half Day Electron-Accelerator Irradiations of Enriched Mo-100 Targets for the Production of Mo-99,” ANL report ANL/NE-16/27. Argonne National Laboratory (2016).

[3] K. Woloshun, G. Dale, E. Olivas, F. Romero, D. Dalmas, S. Chemerisov, R. Gromov, and R. Lowden, “Thermal Test on Target with Pressed Disks,” LANL report LA-UR-16-22211. Los Alamos National Laboratory (2016).

[4] M. Virgo, S. Chemerisov, R. Gromov, C. Jonah, and G. F. Vandegrift, “Results of Thermal Test of Metallic Molybdenum Disk Target and Fast Acting Valve Testing,” ANL report ANL/NE-16/44. Argonne National Laboratory (2016).
[5] K. Woloshun, G. Dale, E. Olivas, A. Naranjo, and F. Romero, “29 mm Diameter Test Target Design Report,” LANL report LA-UR-16-27128. Los Alamos National Laboratory (2016).
[6] K. Woloshun, G. Dale, E. Olivas, A. Naranjo, F. Romero, S. Chemerisov, and R. Gromov, “29 mm Diameter Target Test Report” LANL report LA-UR-17-29718. Los Alamos National Laboratory (2017).
[7] AFT ARROW, Release 4.0, 2012. Applied Flow Technology, Inc., Colorado Springs, CO.
[8] ANSYS CFX, Release 19.2, 2018. Ansys, Inc., Canonsburg, PA.

Appendix
Thermal Hydraulic "MathCad" hand calculations

Helium properties at operating conditions

$p_{atm} := 14.7psi$ Atmospheric pressure

$p_{op} := 300psi$ He operating pressure $p_{op} = 2.068 \times 10^{6} Pa$

$\rho_{HeAtm} := 0.01 \frac{lb}{ft^3}$ He density at STP

$\rho_{op} := \rho_{HeAtm} \cdot \frac{p_{op}}{p_{atm}} = 3.269 \frac{kg}{m^3}$ He density at operating pressure
Table chk @ 20bar = 3.18kg/m^3

$p_{bar} := \frac{p_{op}}{p_{atm}} = 20.408$ Operating pressure in bars

$k_{He} := 0.153 \frac{W}{m \cdot K}$

$k_{He} = 0.088 \cdot \frac{Btu}{hr \cdot ft \cdot R}$ Thermal conductivity of He

$Pr_{He} := 0.7$ From table - constant wrt pressure

$\mu_{He} := 186 \cdot 10^{-7} \frac{N \cdot s}{m^2}$

$\mu_{He} = 1.25 \times 10^{-5} \cdot \frac{lbm}{ft \cdot s}$ Dynamic viscosity of He $\mu_{He} = 1.86 \times 10^{-5} \cdot Pa \cdot s$

$\nu_{He} := \frac{\mu_{He}}{\rho_{op}} = 6.124 \times 10^{-5} \cdot \frac{ft^2}{s}$ Kinematic viscosity of He at operating pressure

$Cp_{He} := \frac{Pr_{He} \cdot k_{He}}{\mu_{He}} = 1.375 \cdot \frac{Btu}{lb \cdot R}$ $Cp_{He} = 5.758 \times 10^{3} \cdot \frac{J}{kg \cdot K}$

Channel geometry

$w_{chn} := 0.71mm$ Channel width

$N_{chn} := 11$ Number of channels

$L_{chn} := 29mm$ Channel height

$D_{chn} := 2 \cdot w_{chn} = 1.42 \cdot mm$ Hydraulic diameter of channel

$Ax_{chn} := w_{chn} \cdot L_{chn} = 20.59 \cdot mm^2$ Cross sectional area of channel

Channel flow conditions

$M_{flow} := 92 \frac{gm}{s}$ Total mass flow rate

$v_{chn} := \frac{M_{flow}}{\rho_{op} \cdot Ax_{chn} \cdot N_{chn}} = 124.255 \frac{m}{s}$ Average He flow velocity in each channel

$Re_{chn} := \frac{v_{chn} \cdot D_{chn}}{\nu_{He}} = 3.101 \times 10^{4}$ Reynolds number > 10,000, turbulent flow

$Nu_{chn} := 0.023 \cdot Re_{chn}^{.8} \cdot Pr_{He}^{.33} = 80.135$ Nusselt number for turbulent flow

$h_{chn} := \frac{Nu_{chn} \cdot k_{He}}{D_{chn}} = 1.521 \times 10^{3} \cdot \frac{Btu}{hr \cdot ft^{2} \cdot \Delta°F}$

$h_{chn} = 0.863 \cdot \frac{W}{cm^{2} \cdot \Delta°C}$ Thermal convective coefficient from classic correlation

Heat Transfer

$q_{12} := 0.177 \frac{kW}{cm^{3} \cdot kW}$ Internal heat generation in center of window
Song's data from Phil's window study for Inconel at 12mm FWHM 40Mev

$q_6 := \left(\frac{12}{6}\right)^{2} \cdot q_{12} = 0.708 \cdot \frac{kW}{cm^{3} \cdot kW}$ Heat generation adjusted for 6mm FWHM beam

$q_{6ad} := q_6 = 0.708 \cdot \frac{kW}{cm^{3} \cdot kW}$ Heat generation adjusted for Mev from 40Mev

$q_{6ad} = 7.08 \times 10^{8} \cdot \frac{W}{m^{3} \cdot kW}$

$P_{BeamTest} := 12kW$ Beam power from test

$q_{6Beam} := P_{BeamTest} \cdot q_{6ad} = 8.496 \times 10^{9} \cdot \frac{W}{m^{3}}$ Heat generation adjusted for beam power

$t_{win} := 0.015in$ Thickness of window at center

$T_{He} := 27\,°C$ He coolant temperature

$q_{winFlux} := t_{win} \cdot q_{6Beam} = 3.237 \times 10^{6} \cdot \frac{W}{m^2}$ Heat flux to coolant at center

$\Delta T_{chn} := \frac{q_{winFlux}}{h_{chn}} = 374.899 \cdot \Delta°C$ Temperature differential between coolant side surface of window and coolant using h as calculated above

$T_{chnHe} := T_{He} + \Delta T_{chn} = 401.899 \cdot °C$ Temperature of coolant side surface of window

$k_{Inc} := 12 \frac{Btu}{hr \cdot ft \cdot \Delta°F}$ Thermal conductivity of Inconel window att 500C

$\Delta T_{win} := \frac{q_{6Beam} \cdot t_{win}^{2}}{2 \cdot k_{Inc}} = 29.691 \cdot \Delta°C$ Temperature differential across Inconel window 1-D heat transfer

$T_{chnBeam} := T_{chnHe} + \Delta T_{win} = 431.59 \cdot °C$ Temperature of beam side surface of window

From CFX Model results Comparison

$T_{cfxHe} := 762K$ $T_{cfxHe} = 488.85 \cdot °C$ Temperature of coolant side surface of window

$T_{chnHeComp} := T_{chnHe} = 401.899 \cdot °C$ Compared to Calc

$T_{cfxBeam} := 803K$ $T_{cfxBeam} = 529.85 \cdot °C$ Temperature of beam side surface of window

$T_{chnBeamComp} := T_{chnBeam} = 431.59 \cdot °C$ Compared to Calc

$\Delta T_{cfxwin} := T_{cfxBeam} - T_{cfxHe} = 41 \cdot \Delta°C$ Temperature differential across Inconel window from cfx

$\Delta T_{winComp} := \Delta T_{win} = 29.691 \cdot \Delta°C$ Compared to Calc

$\Delta T_{cfxh} := T_{cfxHe} - T_{He} = 461.85 \cdot \Delta°C$ Temperature differential between coolant side surface of window and coolant from cfx

$\Delta T_{chnComp} := \Delta T_{chn} = 374.899 \cdot \Delta°C$ Compared to Calc

$$q_{cfxFlux} := 3.18 \cdot 10^{6} \frac{W}{m^{2}}$$

Heat flux to coolant from the CFX

$$q_{winFluxComp} := q_{winFlux} = 3.237 \times 10^{6} \cdot \frac{W}{m^{2}}$$

Compared to Calc

$$h_{cfx} := \frac{q_{cfxFlux}}{\Delta T_{cfxh}} = 0.689 \cdot \frac{W}{cm^{2} \cdot \Delta °C}$$

Thermal convective coefficient using cfx flux from above

$$h_{chnComp} := h_{chn} = 0.863 \cdot \frac{W}{cm^{2} \cdot \Delta °C}$$

Compared to Calc

$$\rho_{cfxHe} := 3.22 \frac{kg}{m^{3}}$$

Density average from cfx

$$\rho_{opComp} := \rho_{op} = 3.269 \frac{kg}{m^{3}}$$

Compared to Calc

$$Cp_{cfxHe} := 5.240 \cdot 10^{3} \cdot \frac{J}{kg \cdot \Delta °C}$$

Heat capacity average from cfx

$$Cp_{HeComp} := Cp_{He} = 5.758 \times 10^{3} \cdot \frac{J}{kg \cdot \Delta °C}$$

Compared to Calc

$$k_{cfxHe} := 0.1415 \frac{W}{m \cdot \Delta °C}$$

Conductivity average from cfx

$$k_{HeComp} := k_{He} = 0.153 \cdot \frac{W}{m \cdot \Delta °C}$$

Compared to Calc

$$\mu_{cfxHe} := 1.86 \cdot 10^{-5} Pa \cdot s$$

Dynamic viscosity average from cfx

$$\mu_{HeComp} := \mu_{He} = 1.86 \times 10^{-5} \cdot Pa \cdot s$$

Compared to Calc

$$Pr_{cfxHe} := \frac{Cp_{cfxHe} \cdot \mu_{cfxHe}}{k_{cfxHe}} = 0.689$$

Prandtl No. average from cfx

$$Pr_{HeComp} := Pr_{He} = 0.7$$

Compared to Calc

$$\nu_{cfxHe} := \frac{\mu_{cfxHe}}{\rho_{cfxHe}} = 5.776 \times 10^{-6} \frac{m^2}{s}$$ Kinematic viscosity average from cfx

$$\nu_{HeComp} := \nu_{He} = 5.69 \times 10^{-6} \frac{m^2}{s}$$ Compared to Calc

$$v_{cfx} := 126 \frac{m}{s}$$ Velocity average through channel input to cfx

$$v_{chnComp} := v_{chn} = 124.255 \frac{m}{s}$$ Compared to Calc

$$Re_{cfx} := \frac{v_{cfx} \cdot D_{chn}}{\nu_{cfxHe}} = 3.097 \times 10^{4}$$ Reynolds average in channel from cfx

$$Re_{chnComp} := Re_{chn} = 3.101 \times 10^{4}$$ Compared to Calc

$$Nu_{cfx} := 0.023 \cdot Re_{cfx}^{0.8} \cdot Pr_{cfxHe}^{0.33} = 79.634$$ Nusselt No. average in channel from cfx

$$Nu_{chnComp} := Nu_{chn} = 80.135$$ Compared to Calc

$$h_{cfxComp} := \frac{Nu_{cfx} \cdot k_{cfxHe}}{D_{chn}} = 0.794 \cdot \frac{W}{cm^2 \cdot \Delta°C}$$ Convective Coefficent average in channel as calculated from properties from cfx

$$h_{chnCorComp} := \frac{Nu_{chn} \cdot k_{He}}{D_{chn}} = 0.863 \cdot \frac{W}{cm^2 \cdot \Delta°C}$$ Compared to Calc

$$h_{ratio} := \frac{h_{chn}}{h_{cfx}} = 1.254$$ Ratio of h calculated to cfx output

$$\Delta T_{rarion} := \frac{\Delta T_{cfxh}}{\Delta T_{chn}} = 1.232$$ Ratio of temperature differences between wall and He of cfx output to calculated

Old 12mm Window thermal test on 5/2/19 at 40Mev 6mm FWHM

Helium properties at operating conditions

$p_{atm} := 14.7psi$ Atmospheric pressure

$p_{op} := 315psi$ He operating pressure $p_{op} = 2.172 \times 10^{6} Pa$

$\rho_{HeAtm} := 0.01 \frac{lb}{ft^3}$ He density at STP

$\rho_{op} := \rho_{HeAtm} \cdot \frac{p_{op}}{p_{atm}} = 3.433 \frac{kg}{m^3}$ He density at operating pressure
Table chk @ 20bar = 3.18kg/m^3

$p_{bar} := \frac{p_{op}}{p_{atm}} = 21.429$ Operating pressure in bars

$k_{He} := 0.153 \frac{W}{m \cdot K}$

$k_{He} = 0.088 \cdot \frac{Btu}{hr \cdot ft \cdot R}$ Thermal conductivity of He

$Pr_{He} := 0.7$ From table - constant wrt pressure

$\mu_{He} := 186 \cdot 10^{-7} \frac{N \cdot s}{m^2}$

$\mu_{He} = 1.25 \times 10^{-5} \cdot \frac{lbm}{ft \cdot s}$ Dynamic viscosity of He $\mu_{He} = 1.86 \times 10^{-5} \cdot Pa \cdot s$

$\nu_{He} := \frac{\mu_{He}}{\rho_{op}} = 5.833 \times 10^{-5} \cdot \frac{ft^2}{s}$ Kinematic viscosity of He at operating pressure

$Cp_{He} := \frac{Pr_{He} \cdot k_{He}}{\mu_{He}} = 1.375 \cdot \frac{Btu}{lb \cdot R}$ $Cp_{He} = 5.758 \times 10^{3} \cdot \frac{J}{kg \cdot K}$

Channel geometry

$w_{chn} := 0.02in$ Channel width

$N_{chn} := 28$ Number of channels

26+2 more channels accounts for wider channels at back

$L_{chn} := 10.16mm$ Channel height

$D_{chn} := 2 \cdot w_{chn} = 1.016 \cdot mm$ Hydraulic diameter of channel

$Ax_{chn} := w_{chn} \cdot L_{chn} = 5.161 \cdot mm^2$ Cross sectional area of channel

Channel flow conditions

$M_{flow} := 136 \frac{gm}{s}$ Total mass flow rate

$M_{chn} := \frac{M_{flow}}{N_{chn}} = 4.857 \cdot \frac{gm}{s}$ Mass flow per channel

$v_{chn} := \frac{M_{flow}}{\rho_{op} \cdot Ax_{chn} \cdot N_{chn}} = 274.163 \frac{m}{s}$ Average He flow velocity in each channel

$v_{chn} = 899.486 \cdot \frac{ft}{s}$

$Re_{chn} := \frac{v_{chn} \cdot D_{chn}}{\nu_{He}} = 5.14 \times 10^4$ Reynolds number > 10,000, turbulent flow

$Nu_{chn} := 0.023 \cdot Re_{chn}^{.8} \cdot Pr_{He}^{.33} = 120.064$ Nusselt number for turbulent flow

$h_{chn} := \frac{Nu_{chn} \cdot k_{He}}{D_{chn}} = 3.184 \times 10^3 \cdot \frac{Btu}{hr \cdot ft^2 \cdot \Delta°F}$

Thermal convective coefficient

$h_{chn} = 1.808 \cdot \frac{W}{cm^2 \cdot \Delta°C}$

$h_{chn} = 1.808 \times 10^4 \cdot \frac{W}{m^2 \cdot K}$

Heat Transfer

$q_{12} := 0.177 \frac{kW}{cm^3 \cdot kW}$ Internal heat generation in center of window
Song's data from Phil's window study for Inconel at
12mm FWHM 40Mev

$q_6 := \left(\frac{12}{6}\right)^2 \cdot q_{12} = 0.708 \cdot \frac{kW}{cm^3 \cdot kW}$ Heat generation adjusted for 6mm FWHM beam

$q_{6ad} := \frac{40}{40} \cdot q_6 = 0.708 \cdot \frac{kW}{cm^3 \cdot kW}$ Heat generation adjusted for 40Mev

$q_{6ad} = 7.08 \times 10^8 \cdot \frac{W}{m^3 \cdot kW}$

$P_{BeamTest} := 20kW$ Beam power from test

$q_{6Beam} := P_{BeamTest} \cdot q_{6ad} = 1.416 \times 10^{10} \cdot \frac{W}{m^3}$ Heat generation adjusted for beam power

$t_{win} := 0.015in$ Thickness of window at center

$T_{He} := 27\,°C$ He coolant temperature

$\Delta T_{chn} := \frac{t_{win} \cdot q_{6Beam}}{h_{chn}} = 298.385 \cdot \Delta°C$ Temperature differential between coolant side surface of window and coolant using h as calculated above

$T_{chnHe} := T_{He} + \Delta T_{chn} = 325.385 \cdot °C$ Temperature of coolant side surface of window

$k_{Inc} := 12 \frac{Btu}{hr \cdot ft \cdot \Delta°F}$ Thermal conductivity of Inconel window att 500C

$\Delta T_{win} := \frac{q_{6Beam} \cdot t_{win}^2}{2 \cdot k_{Inc}} = 49.485 \cdot \Delta°C$ Temperature differential across Inconel window
1-D heat transfer

$T_{chnBeam} := T_{chnHe} + \Delta T_{win} = 374.87 \cdot °C$ Temperature of beam side surface of window

This page intentionally left blank.

Experimental Operations and Facilities Division
Argonne National Laboratory
9700 South Cass Avenue, Bldg. 205
Argonne, IL 60439-4832

www.anl.gov